Dark-bright solitons and their lattices in atomic Bose-Einstein condensates

D. Yan,[1] F. Tsitoura,[2] P. G. Kevrekidis,[1] and D. J. Frantzeskakis[2]
[1]*Department of Mathematics and Statistics, University of Massachusetts, Amherst, Massachusetts 01003-4515, USA*
[2]*Department of Physics, University of Athens, Panepistimiopolis, Zografos, Athens 15784, Greece*
(Received 8 February 2014; revised manuscript received 13 January 2015; published 20 February 2015)

In the present contribution, we explore a host of different stationary states, namely dark-bright solitons and their lattices, that arise in the context of multicomponent atomic Bose-Einstein condensates. The latter are modeled by systems of coupled Gross-Pitaevskii equations with general interaction (nonlinearity) coefficients g_{ij}. It is found that in some particular parameter ranges such solutions can be obtained in analytical form, however, numerically they are computed as existing in a far wider parametric range. Many features of the solutions under study, such as their analytical form without the trap or the stability and dynamical properties of one dark-bright soliton even in the presence of the trap are obtained analytically and corroborated numerically. Additional features, such as the stability of soliton lattice homogeneous states or their existence and stability in the presence of the trap, are examined numerically.

DOI: 10.1103/PhysRevA.91.023619 PACS number(s): 03.75.Mn, 05.45.Yv, 03.75.Kk

I. INTRODUCTION

Dark-bright (DB) solitons constitute exact solutions of the completely integrable, defocusing, two-component Manakov model [1], i.e., the vector variant of the nonlinear Schrödinger equation [2]. These structures exist in the presence of equal nonlinear interactions within and between components. As such, they can be thought of as symbiotic structures, since the bright components thereof would not be sustainable in defocusing settings, and only emerge because of the effective potential well created by the dark soliton component through the interspecies interaction.

Taking advantage of the ratios of inter- and intraspecies interactions between Bose-condensed hyperfine spin states of atomic ^{87}Rb, being very proximal to unity, dark-bright solitons were proposed as being experimentally relevant in atomic Bose-Einstein condensates (BECs) even since 2001 [3]. However, this possibility was at a somewhat dormant stage until 2008, when the Hamburg group was able to produce experimentally such coherent structures using phase-imprinting techniques [4], and to illustrate their robustness in ^{87}Rb BECs. The above mentioned as well as subsequent efforts revealed a number of exciting characteristics of these nonlinear entities. For instance, it was shown that DB solitary waves oscillate in a trap with a reduced frequency in comparison to their dark single-component counterparts due to the presence of the bright filling component [3–5]. Dark-bright soliton trains were created by inducing counterflow between two miscible BECs past a critical velocity [6]. Molecules of a few DB solitary waves were observed in related experiments, and offered the seed for detailed investigations of the interactions between DB solitons [7–9]. Furthermore, beating (in time) dark-dark solitons, which turn out to be SO(2) rotated versions of DB solitons were also predicted and observed in experiments [10,11], further adding to the richness of this multicomponent setting. In addition, the interaction of such states with potential barriers was experimentally explored [12]. It should also be noted that two-dimensional generalizations of these structures have been considered, both in the context of dark-bright rings [13] and in that of vortex-bright solitary waves [14,15].

Our aim in the present work is to present a set of analytical solutions and numerical results both for individual DB solitary waves and also for lattices of such waves, for arbitrary nonlinear coefficients (within suitable bounds). This is relevant for a number of reasons not only theoretically, but also experimentally. On the one hand, not all atomic species have as nearly equal inter- and intraspecies interaction scattering length, as is the case with Rubidium. Perhaps even more importantly, the now well-established technique of Feshbach resonance [16] (see also Refs. [17] for work in two-component BECs) can be used to detune the nonlinear coefficients from this degenerate case of equal strength and, thus, it is relevant to appreciate the potential robustness (or lack thereof) of these nonlinear waves in such settings.

We start by presenting DB solitary waves in explicit analytical form and identify the algebraic conditions that need to be satisfied for the relevant solutions to exist. We solve such algebraic equations for the characteristic properties of the solutions and offer an interpretation of the resulting expressions. In addition, we extract conditions under which such families of solutions will be possible to sustain. In addition to identifying the relevant solutions in explicit numerical computations, we are able to more importantly establish their potential existence and robustness in the experimentally relevant setting of trapped binary condensates. Whenever possible, our considerations will be fully analytical. Examples of this type will concern, e.g., the explicit form of the DB solitary waves and their lattices for general coefficients, or the analysis of the motion of a single DB for general interactions in the presence of the trap. However, other aspects of our considerations, such as the stability of the lattices of such waves in either the homogeneous or the trapped state will be developed by numerical methods. The combination of both types of tools will provide us with a broad understanding of the existence, stability, and dynamical properties of the single DB solitary waves and their multiple DB generalizations as a function of the nonlinear interatomic interaction strengths.

We should note that although in the BEC literature, we are not aware of any investigations along these analytical lines (the closest analysis which offers numerical borders of existence

of single dark-bright solitons consists of the work of [18]); in the optics literature, there are some similar studies that we now highlight. First, it should be noted that these cases do not consider the framework of a harmonic trap, which is less physically relevant in that context. A study of DB solitary waves for general coefficients has been conducted in the work of [19], while periodic solutions, yet solely for the limit of equal nonlinear interactions were obtained in [20].

Our presentation will be structured as follows: In Sec. II, we will provide the relevant model setup and present the well-known DB soliton solutions, as introduced in the Manakov limit (see, e.g., Ref. [3]). We will also explore lattices of such solitary waves in the homogeneous case near that limit and present our analytical results for the stability and motion of a single DB solitary wave in the presence of the trap. In Sec. III, we present our numerical considerations, confirming the existence of both single and multiple DB solitary wave solutions, both in the vicinity, as well as far from the Manakov limit, both in the absence, as well as in the presence of the parabolic trap confining the atoms. Finally, in Sec. IV, we summarize our findings and propose some challenges for future work.

II. MODEL SETUP AND ANALYTICAL CONSIDERATIONS

We commence our analysis by considering a two-component elongated (along the x direction) repulsive BEC, composed of two different hyperfine states of the same alkali-metal isotope. We focus on the experimentally tractable setting of a highly anisotropic trap, i.e., the longitudinal and transverse trapping frequencies are such that $\omega_x \ll \omega_\perp$. In this case, the system at hand can be described at the mean-field level by two coupled Gross-Pitaevskii equations (GPEs) of the form [21],

$$i\hbar\partial_t\psi_j = \left(-\frac{\hbar^2}{2m}\partial_x^2\psi_j + V(x) - \mu_j + \sum_{k=1}^{2} g_{jk}|\psi_k|^2\right)\psi_j. \tag{1}$$

In this model, $\psi_j(x,t)$ $(j = 1,2)$ denote the mean-field wave functions of the two components (normalized to the numbers of atoms $N_j = \int_{-\infty}^{+\infty}|\psi_j|^2dx$), m is the atomic mass, and μ_j are the chemical potentials; furthermore, $g_{jk} = 2\hbar\omega_\perp a_{jk}$ are the effective one-dimensional (1D) coupling constants, with a_{jk} denoting the three s-wave scattering lengths ($a_{12} = a_{21}$) which account for collisions between atoms belonging to the same (a_{jj}) or different ($a_{jk}, j \neq k$) species. The external trapping potential is parabolic, of the form $V(x) = (1/2)m\omega_x^2x^2$. Introducing normalized densities $|u_j|^2 = 2a|\psi_j|^2$, and measuring length, time, and energy in units of $a_\perp = \sqrt{\hbar/(m\omega_\perp)}$, $\omega_\perp^{-1}$ and $\hbar\omega_\perp$, respectively, Eq. (1) is expressed in the following dimensionless form:

$$i\partial_t u_1 = -\tfrac{1}{2}\partial_x^2u_1 + V(x)u_1 + (g_{11}|u_1|^2 + g_{12}|u_2|^2 - \mu_1)u_1, \tag{2}$$

$$i\partial_t u_2 = -\tfrac{1}{2}\partial_x^2u_2 + V(x)u_2 + (g_{12}|u_2|^2 + g_{22}|u_1|^2 - \mu_2)u_2. \tag{3}$$

The normalized external potential in Eqs. (2) and (3) assumes the form,

$$V(x) = \tfrac{1}{2}\Omega^2x^2, \tag{4}$$

where $\Omega = \omega_x/\omega_\perp$ represents the normalized trap strength.

It is important to note here that from the point of view of BEC applications, we are considering a regime where, typically, the two-component system will bear a few thousand atoms. Such a consideration is necessary in order to ensure that quantum fluctuations can be neglected: Indeed, in such a case, the recent works [22,23] for dark and bright solitons, respectively, clearly suggest that the role of quantum fluctuations should be negligible—cf. in particular Fig. 5 of Ref. [22] and Fig. 6 of Ref. [23]. The latter clearly illustrates that the uncertainty in the position and momenta of the wave rapidly approaches its saturation value for a little over 1000 atoms. In that respect, in the numerical results that we present below, we consider the case of a ^{87}Rb BEC mixture (of atomic mass $m = 144 \times 10^{-27}$ kg and scattering lengths $a_{ij} \approx 100a_0$, where a_0 is the Bohr radius) and use the following parameter values: normalized trap strengths $\Omega = 0.1$ or $\Omega = 0.02$ (corresponding to a longitudinal trapping frequency $\omega_x = 2\pi \times 8$ Hz and transverse trapping frequencies $\omega_\perp = 2\pi \times 80$ Hz and $\omega_\perp = 2\pi \times 400$ Hz, respectively), as well as normalized chemical potentials $\mu_{1,2}$ $(j = 1,2)$ and scattering lengths g_{ij} $(i,j = 1,2)$ of order unity. For such a choice, the number of atoms of the condensate ranges, approximately, from 4000 to 9000, for $\Omega = 0.1$ and $\Omega = 0.02$, respectively. Hence, within our operating parameters, the mean-field description is a quite relevant one for the corresponding BEC system.

A. Single DB soliton in the homogeneous system

We will now illustrate that solitary waves of the DB type can in fact be found in an explicit analytical form even outside of the very special integrable regime of $g_{ij} = 1$, where inverse scattering theory provides such explicit solutions [2]. To that effect, we will consider the analytically tractable case of $V(x) = 0$ (and subsequently illustrate how our results are modified in the presence of a trap) in Eqs. (2) and (3), but maintain as general coefficients as possible; namely g_{ij} will be arbitrary and will only be constrained by the conditions for the existence of our solutions in what follows.

We now seek real, standing-wave solutions of Eqs. (2) and (3), with $\partial_t u_j = 0$, and obtain

$$\mu_1u_1 = -\tfrac{1}{2}u_1'' + \left(g_{11}u_1^2 + g_{12}u_2^2\right)u_1, \tag{5}$$

$$\mu_2u_2 = -\tfrac{1}{2}u_2'' + \left(g_{12}u_1^2 + g_{22}u_2^2\right)u_2, \tag{6}$$

where primes denote differentiation with respect to x. We now try explicit analytical solutions in the form of a dark (black) solitary wave for u_1 and a bright solitary wave for u_2, namely,

$$u_1 = A_1\tanh(bx), \tag{7}$$

$$u_2 = A_2\mathrm{sech}(bx), \tag{8}$$

where A_1 and A_2 denote the amplitudes of the dark and bright component, respectively, while b stands for the common inverse width. Inserting the above expressions into the equations

of motion, we find that the latter are satisfied provided that a number of algebraic conditions hold. More specifically, to satisfy Eq. (5), we need

$$\mu_1 = b^2 + g_{12}A_2^2, \tag{9}$$

$$b^2 = g_{11}A_1^2 - g_{12}A_2^2, \tag{10}$$

while to satisfy Eq. (6), we need to have

$$\mu_2 = -\frac{b^2}{2} + g_{12}A_1^2, \tag{11}$$

$$b^2 = g_{12}A_1^2 - g_{22}A_2^2. \tag{12}$$

We can now suggest a simple way to view the relevant solvability conditions: One can solve Eqs. (9), (10), and (12) as three linear equations in three unknowns (A_1^2, A_2^2, and b^2), provided that the interactions strengths g_{ij} and the chemical potential μ_1 are set. Then, the remaining Eq. (11) can be used as a closure condition, self-consistently determining the chemical potential of the second (bright) component. In this viewpoint, the analytical solution at hand has the amplitude parameters A_1 and A_2 determined as

$$A_1^2 = \frac{\mu_1}{g_{11}}, \tag{13}$$

$$A_2^2 = \frac{\mu_1}{g_{11}}\frac{g_{11}-g_{12}}{g_{12}-g_{22}}, \tag{14}$$

and the inverse width parameter b is determined by

$$b^2 = \frac{\mu_1}{g_{11}}\frac{g_{11}g_{22}-g_{12}^2}{g_{22}-g_{12}}, \tag{15}$$

while Eq. (11), with input from (15) and (13) completes the calculation.

Some important—and physically relevant—conclusions can be already drawn by this calculation about the nature of the exact solitary waves obtained through the above calculation and the constraints on the existence parameters. In particular, it can be directly seen from Eq. (14) that the bright component can only exist when

$$\min(g_{11},g_{22}) < g_{12} < \max(g_{11},g_{22}). \tag{16}$$

Furthermore, it is interesting to also infer from Eq. (15) that if $g_{22} > g_{12}$ (i.e., the second component possesses the largest scattering length, while the dark soliton is in the first component), then such exact DB solitons will *only* exist for miscible components, namely for $g_{11}g_{22} > g_{12}^2$. On the other hand, if $g_{22} < g_{12}$ (i.e., if the first component possesses the largest scattering length *and* is the one holding the dark soliton), then the above explicit DB solitons will solely exist for immiscible components, i.e., for $g_{11}g_{22} < g_{12}^2$.

B. Lattices of DB solitons

We now consider two types of lattice generalizations of the relevant single DB soliton solutions. In the first one, the dark solitons generalize into the form of a Jacobi elliptic function solution of the sn-type, while the bright solitons generalize into a cn-type solution. This suggests that the adjacent solitary waves in this structure are out-of-phase with respect to each other. In the second generalization, while the dark solitons preserve the same type of structure, the bright ones are now of the dn-type, amounting to in-phase bright solitons in the second component.

1. DB soliton lattice with out-of-phase bright neighbors

In this case, for the system of Eqs. (5) and (6), we use the ansatz of the form,

$$u_1 = A_1\mathrm{sn}(bx,k), \tag{17}$$

$$u_2 = A_2\mathrm{cn}(bx,k), \tag{18}$$

where k is the elliptic modulus. In this case, the two resulting algebraic equations stemming from Eq. (5) read

$$\mu_1 = \frac{1+k^2}{2}b^2 + g_{12}A_2^2, \tag{19}$$

$$k^2b^2 = g_{11}A_1^2 - g_{12}A_2^2. \tag{20}$$

Similarly, the conditions stemming from Eq. (6) are

$$\mu_2 = \frac{1-2k^2}{2}b^2 + g_{12}A_1^2, \tag{21}$$

$$k^2b^2 = g_{12}A_1^2 - g_{22}A_2^2. \tag{22}$$

It is interesting to observe that the special limit case of the hyperbolic functions, namely $k \to 1$, naturally asymptotes to the single DB equations' limit of Eqs. (9)–(12). The other relevant limit is the trigonometric one of $k \to 0$, which provides sinusoidal and cosinusoidal solutions, respectively, for the two components; nevertheless, direct inspection of the equations illustrates that this is so only at the transition threshold between miscibility and immiscibility (since it can be directly inferred that such solutions only exist for $g_{11}g_{22} = g_{12}^2$).

Once again, assuming that Eqs. (19), (20), and (22) constitute a linear system for A_1^2, A_2^2, and b^2, while Eq. (21) determines μ_2 (for fixed μ_1 and g_{ij}), we find the amplitudes:

$$A_1^2 = \frac{2k^2(g_{12}-g_{22})\mu_1}{\left(g_{12}^2-g_{11}g_{22}\right)+k^2\left(2g_{11}g_{12}-g_{12}^2-g_{11}g_{22}\right)}, \tag{23}$$

$$A_2^2 = \frac{2k^2(g_{11}-g_{12})\mu_1}{\left(g_{12}^2-g_{11}g_{22}\right)+k^2\left(2g_{11}g_{12}-g_{12}^2-g_{11}g_{22}\right)}, \tag{24}$$

while the (inverse) width parameter b is given by

$$b^2 = \frac{2\left(g_{11}g_{22}-g_{12}^2\right)\mu_1}{\left(g_{12}^2-g_{11}g_{22}\right)+k^2\left(2g_{11}g_{12}-g_{12}^2-g_{11}g_{22}\right)}. \tag{25}$$

It is again relevant to attempt to extract the conditions under which these solutions exist. In particular, the product of Eqs. (23) and (24) yields that Eq. (16) is still valid. The product of each of Eqs. (23) and (24) with Eq. (25) yields once again the conclusion that for the lattice solutions to exist the following must be true: If the dark soliton lattice is in the component with the smaller scattering length, the hyperfine states need to be miscible (i.e., for $g_{11} < g_{12} < g_{22}$, it must be $g_{12}^2 < g_{11}g_{22}$). On the other hand, if the dark lattice is in the component with the larger scattering length, then the states should be immiscible (i.e., for $g_{22} < g_{12} < g_{11}$, it must be $g_{12}^2 > g_{11}g_{22}$). Nevertheless, an additional, more complex condition emerges from the denominator $D_e = (g_{12}^2 - g_{11}g_{22}) + k^2(2g_{11}g_{12} - g_{12}^2 - g_{11}g_{22})$ of the expressions of Eq. (23)–(25). In particular,

for $g_{11} < g_{12} < g_{22}$, it must be that $D_e < 0$, while for $g_{22} < g_{12} < g_{11}$, the opposite must be true, namely $D_e > 0$. By considering this denominator as a binomial in g_{12}, it is clear that g_{12} should be outside the interval of its roots for $D_e > 0$ and inside the same interval for $D_e < 0$.

It is important to note here that no constraint has, *a priori*, been placed on the additional parameter, i.e., the elliptic modulus k appearing in the equations above, aside from the requirement that $D_e < 0$ or $D_e > 0$, depending on the ordering of the scattering lengths. Nevertheless, k is a crucial parameter since it controls the separation between the solitary waves, which for the above solution is given by $s = 2K(k)/b$, where K denotes the complete elliptic integral of the first kind.

2. DB soliton lattice with in-phase bright neighbors

We now consider the case where the first component still has the same profile as in the previous lattice example, namely $u_1 = A_1 \mathrm{sn}(bx,k)$, while the second component has the form,

$$u_2 = A_2 \mathrm{dn}(bx,k). \tag{26}$$

In this case, the solvability conditions from Eq. (5) become

$$\mu_1 = \frac{1+k^2}{2} b^2 + g_{12} A_2^2, \tag{27}$$

$$k^2 b^2 = g_{11} A_1^2 - k^2 g_{12} A_2^2, \tag{28}$$

while those stemming from Eq. (6) acquire the form,

$$\mu_2 = \frac{2-k^2}{2} b^2 + \frac{g_{12}}{k^2} A_1^2, \tag{29}$$

$$k^2 b^2 = g_{12} A_1^2 - k^2 g_{22} A_2^2. \tag{30}$$

Once again the hyperbolic function limit $k \to 1$ yields the familiar form of the DB solitary wave solvability conditions. In this case, the trigonometric limit $k \to 0$ does not represent a multicomponent solution.

Solving in the familiar way Eqs. (27), (28), and (30), we obtain the amplitudes,

$$A_1^2 = \frac{2k^2(g_{12}-g_{22})\mu_1}{2g_{11}g_{12} - g_{12}^2 - g_{11}g_{22} + k^2\left(g_{12}^2 - g_{11}g_{22}\right)}, \tag{31}$$

$$A_2^2 = \frac{2k^2(g_{11}-g_{12})\mu_1}{2g_{11}g_{12} - g_{12}^2 - g_{11}g_{22} + k^2\left(g_{12}^2 - g_{11}g_{22}\right)}, \tag{32}$$

while the inverse width b parameter is obtained by

$$b^2 = \frac{2\left(g_{12}^2 - g_{11}g_{22}\right)\mu_1}{2g_{11}g_{12} - g_{12}^2 - g_{11}g_{22} + k^2\left(g_{12}^2 - g_{11}g_{22}\right)}. \tag{33}$$

In addition to the constraints of the single DB solitary wave [obtained as in the previous subsection by pairwise multiplication of Eqs. (31)–(33)], an additional constraint stems from the denominator $\tilde{D}_e = 2g_{11}g_{12} - g_{12}^2 - g_{11}g_{22} + k^2(g_{12}^2 - g_{11}g_{22})$, which should be such that if $g_{11} < g_{12} < g_{22}$, then $\tilde{D}_e < 0$, while if $g_{11} > g_{12} > g_{22}$, then $\tilde{D}_e > 0$. Once again, this can be viewed as a binomial in g_{12} with the corresponding condition being translated as a statement about the placement of g_{12} in comparison to its roots. In this case, too, the separation between adjacent solitary waves is controlled by k, with the relevant distance being $s = 2K(k)/b$.

C. Dynamics of a single DB soliton in the trap

Finally, from the point of view of analytical considerations, another case that can be studied is that of the dynamics of a single DB soliton in the presence of a parabolic trap. Here, we will resort to the use of Hamiltonian perturbation theory in order to appreciate the effect of the trap on the soliton dynamics (see, e.g., [7,24] and the review [25]). More specifically, we start by casting Eqs. (2) and (3) into the following form:

$$i\partial_t u_d = -\tfrac{1}{2}\partial_x^2 u_d + V(x)u_d + (|u_d|^2 + \tilde{g}_{12}|u_b|^2 - \mu_d)u_d, \tag{34}$$

$$i\partial_t u_b = -\tfrac{1}{2}\partial_x^2 u_b + V(x)u_b + (\tilde{g}_{12}|u_b|^2 + \tilde{g}_{22}|u_d|^2 - \mu_b)u_b. \tag{35}$$

In the above equations, we have used the notation $u_1 = u_d$ and $u_2 = u_b$ (and also $\mu_1 = \mu_d$ and $\mu_2 = \mu_b$), indicating that the component 1 (2) will be supporting a dark (bright) soliton and $\tilde{g}_{12} = \alpha_{12}/\alpha_{11} = \alpha_{21}/\alpha_{11}$, $\tilde{g}_{22} = \alpha_{22}/\alpha_{11}$. Assuming that the dark soliton is on top of a Thomas-Fermi (TF) cloud characterized by the density $|u_{\mathrm{TF}}|^2 = \mu_d - V(x)$, we may substitute the density $|u_d|^2$ in Eqs. (34) and (35) by $|u_d|^2 \to |u_{\mathrm{TF}}|^2|u_d|^2$ [25]. Furthermore, introducing the transformations $t \to \mu_d t$, $x \to \sqrt{\mu_d}x$, $|u_b|^2 \to \mu_d^{-1}|u_b|^2$, we cast Eqs. (34) and (35) into the form:

$$i\partial_t u_d + \tfrac{1}{2}\partial_x^2 u_d - (|u_d|^2 + \tilde{g}_{12}|u_b|^2 - 1)u_d = R_d, \tag{36}$$

$$i\partial_t u_b + \tfrac{1}{2}\partial_x^2 u_b - (\tilde{g}_{12}|u_d|^2 + \tilde{g}_{22}|u_b|^2 - \tilde{\mu})u_b = R_b, \tag{37}$$

where $\tilde{\mu} = \mu_b/\mu_d$, and the functional perturbations R_d and R_b are given by

$$R_d \equiv \left(2\mu_d^2\right)^{-1}[2(1-|u_d|^2)V(x)u_d + V'(x)\partial_x u_d], \tag{38}$$

$$R_b \equiv \mu_d^{-2}(1 - \tilde{g}_{12}|u_d|^2)V(x)u_b, \tag{39}$$

with $V'(x) \equiv dV/dx$. Equations (36) and (37) can be viewed as a system of two coupled perturbed NLS equations, with perturbations given by Eqs. (38) and (39). In the absence of the perturbations it is clear that Eqs. (36) and (37) possess a stationary single DB soliton [cf. Eqs. (7) and (8)]. However, as we are interested in studying the dynamics of a moving single DB soliton in the trap, it is convenient to consider here another, nonstationary DB soliton solution of Eqs. (36) and (37), which can be expressed as follows (see, e.g., Refs. [3,24] for a similar solution, but in the Manakov limit of $g_{ij} = 1$):

$$u_d(x,t) = \cos\phi \tanh[D(x - x_0(t))] + i\sin\phi, \tag{40}$$

$$u_b(x,t) = \eta \mathrm{sech}[D(x - x_0(t))] \times \exp[ikx + i\theta(t) + i(\tilde{\mu} - 1)t]. \tag{41}$$

Here, ϕ is the dark soliton's phase angle, $\cos\phi$ and η represent the amplitudes of the dark and bright solitons, D and $x_0(t)$ denote the inverse width and the center of the DB soliton, while $k = D\tan\phi = \mathrm{const}$ and $\theta(t)$ are the wave number and phase of the bright soliton, respectively. Notice that the dark soliton

in the above solution may also be a "gray"—i.e., a moving one (for $0 \neq \phi < \pi/2$)—which becomes stationary (black) only in the limiting case of $\phi = 0$. In this limit, the solution of Eqs. (40) and (41) coincides with the one given in Eqs. (7) and (8), with $\mu_1 = \mu_d = 1$, $A_1 = 1$, $A_2 = \eta$, and $b = D$ (along with the normalizations of the nonlinearity coefficients described above).

Inserting Eqs. (40) and (41) into Eqs. (36) and (37), we find that the soliton parameters should satisfy certain conditions—similar to those given in Eqs. (9)–(12). In particular, to satisfy Eq. (36), we need

$$D^2 = \cos^2\phi - \tilde{g}_{12}\eta^2, \tag{42}$$

$$\dot{x}_0 = D\tan\phi, \tag{43}$$

while to satisfy Eq. (6), we need to have

$$D^2 = \tilde{g}_{12}\cos^2\phi - \tilde{g}_{22}\eta^2, \tag{44}$$

$$\theta(t) = \tfrac{1}{2}(D^2 - k^2)t + (1 - \tilde{g}_{12})t. \tag{45}$$

It is clear that the closure conditions of the above equations, namely,

$$\eta^2 = \frac{\tilde{g}_{12} - 1}{\tilde{g}_{22} - \tilde{g}_{12}}, \tag{46}$$

$$D^2 = \frac{\tilde{g}_{22} - \tilde{g}_{12}^2}{\tilde{g}_{22} - \tilde{g}_{12}}, \tag{47}$$

are consistent with Eqs. (14) and (15). We also note that in our considerations below we will use the following equation connecting the number of atoms N_b of the bright soliton with the amplitude η of the bright soliton, the dark-soliton component's chemical potential μ_d, and the inverse width D of the above DB soliton:

$$N_b \equiv \int_{-\infty}^{+\infty} |u_b|^2 dx = \frac{2\sqrt{\mu_d}\eta^2}{D}. \tag{48}$$

Let us now assume that the DB soliton evolves adiabatically in the presence of the small perturbation, and employ the Hamiltonian approach of the perturbation theory for matter-wave solitons to study the DB-soliton dynamics. We start by considering the Hamiltonian (total energy) of the system of Eqs. (36) and (37), when the perturbations are absent ($R_d = R_b = 0$), namely,

$$\begin{aligned} E &= \frac{1}{2}\int_{-\infty}^{+\infty} \mathcal{E} dx, \\ \mathcal{E} &= |\partial_x u_d|^2 + |\partial_x u_b|^2 + (|u_d|^2 - 1)^2 + \tilde{g}_{22}|u_b|^4 \\ &\quad - 2\tilde{\mu}|u_b|^2 + 2\tilde{g}_{12}|u_b|^2|u_d|^2. \end{aligned} \tag{49}$$

The energy of the system, when calculated for the DB-soliton solution of Eqs. (40) and (41), takes the following form:

$$\begin{aligned} E &= \tfrac{4}{3}D^3 + \tfrac{1}{6}\chi D^2(2\tilde{g}_{12} + 3\tan^2\phi + 1) \\ &\quad + \tfrac{1}{6}\chi^2 D\left(\tilde{g}_{22} - \tilde{g}_{12}^2\right) + \chi(\tilde{g}_{12} - \tilde{\mu}), \end{aligned} \tag{50}$$

where $\chi = N_b/\sqrt{\mu_d}$.

Since we have considered an adiabatic evolution of the DB soliton, we may assume that, in the presence of the perturbations of Eqs. (38) and (39), the DB soliton parameters become slowly-varying unknown functions of time t. Thus, the DB soliton parameters become $\phi \to \phi(t)$, $D \to D(t)$, and, as a result, Eqs. (42) and (43) are generalized to read

$$D^2(t) = \cos^2\phi(t) - \tfrac{1}{2}\tilde{g}_{12}\chi D(t), \tag{51}$$

$$\dot{x}_0(t) = D(t)\tan\phi(t), \tag{52}$$

where we have used Eq. (48). The evolution system of the parameters $\phi(t)$, $D(t)$, and $x_0(t)$ can then be closed by means of the evolution of the DB soliton energy. In particular, Eq. (50) with Eqs. (51) and (52) leads to the evolution of the soliton energy, dE/dt. In addition, the latter can be also found using Eqs. (36) and (37) and their complex conjugates, namely,

$$\begin{aligned} \frac{dE}{dt} &= -2\mathrm{Re}\left\{\int_{-\infty}^{+\infty}(R_d^*\partial_t u_d + R_b^*\partial_t u_b)dx\right\} \\ &= \frac{V'(x)}{\mu_d^2}\Bigg[2\sin\phi\cos^3\phi - \frac{2}{3}\tilde{g}_{12}\chi D\sin\phi\cos\phi \\ &\quad - \chi D\tan\phi\left(1 - \tilde{g}_{12}\left(1 - \frac{\cos^2\phi}{3}\right)\right)\Bigg]. \end{aligned} \tag{53}$$

Equating the expressions for dE/dt, we can end up with the following equation, describing the evolution of the DB soliton parameters:

$$\begin{aligned} &4D^2\dot{D} + \frac{1}{3}\chi D\dot{D}(2\tilde{g}_{12} + 3\tan^2\phi + 1) + \chi D^2\tan\phi\sec^2\phi\dot{\phi} + \frac{1}{6}\chi^2\dot{D}\left(\tilde{g}_{22} - \tilde{g}_{12}^2\right) \\ &= \frac{V'(x)}{\mu_d^2}\left[2\sin\phi\cos^3\phi - \frac{2}{3}\tilde{g}_{12}\chi D\sin\phi\cos\phi - \chi D\tan\phi\left(1 - \tilde{g}_{12}\left(1 - \frac{\cos^2\phi}{3}\right)\right)\right]. \end{aligned} \tag{54}$$

The above equation, together with Eqs. (51) and (52), form a system of differential equations describing the evolution of the soliton parameters ϕ, D, and x_0. This system can be solved approximately, upon considering solitons near the center of the trap (i.e., $x_0 \approx 0$), and linearizing around the fixed point at

$$x_0 = 0, \quad \phi_0 = 0, \quad D_0 = \frac{\chi}{4}\tilde{g}_{12}\left(\sqrt{1 + \frac{16}{\chi^2\tilde{g}_{12}^2}} - 1\right). \tag{55}$$

We can now linearize Eqs. (54) and (51) and (52), using the ansatz: $x_0 = X_0$, $\phi = \phi_1$, and $D = D_0 + D_1$. To this end, combining the resulting equation for X_0, ϕ_1, and D_1, we can end up with the following equation of motion for the soliton center:

$$\ddot{X}_0 = -\frac{R}{W}V'(X_0), \tag{56}$$

where

$$R = D_0(2 - \tilde{g}_{12}\chi D_0 + \chi D_0(\tilde{g}_{12} - 1)), \tag{57}$$

$$W = 8D_0^2\tilde{D}_0 - \chi D_0^2 + \tfrac{2}{3}\tilde{D}_0 D_0 \chi(2\tilde{g}_{12} + 1) + \tfrac{1}{3}\chi^2\tilde{D}_0\left(\tilde{g}_{22}^2 - \tilde{g}_{12}^2\right), \tag{58}$$

and $\tilde{D}_0 = \frac{1}{2D_0 + \frac{\chi}{2}\tilde{g}_{12}}$. Note that in the Manakov limit of $\tilde{g}_{12} = \tilde{g}_{22} = 1$, Eq. (56) recovers the equation of motion for the soliton center found in Ref. [3]:

$$\ddot{X}_0 = -\frac{1}{2}V'(X_0) + \frac{N_b}{8\sqrt{\mu + \left(\frac{N_b}{4}\right)^2}}V'(X_0). \tag{59}$$

In the general case of $g_{ij} \neq 1$, Eq. (56) shows that, again, the parabolic trap leads to a restoring linear force, although here it is a considerably more complex one, that depends explicitly on the $\tilde{g}_{ij}$'s. The consequences of this prediction will be further assessed in the next section, where it will be compared to numerical computations.

III. NUMERICAL RESULTS

A. Comparison of numerics with analytics

1. *Dark-bright solitons and lattices thereof in the homogeneous case*

To illustrate the relevance and usefulness of our analysis, we start the presentation of our numerical results by a series of computations that compare the solutions identified numerically with the corresponding analysis presented above for the homogeneous BEC case, where the potential is absent in Eqs. (2) and (3), i.e., $V(x) = 0$. In this context, we have identified numerically exact solutions (up to a prescribed precision typically set to 10^{-7}), using a fixed point iteration scheme of the Newton-Raphson type. In so doing, we have confirmed that our analytical solutions are indeed numerically exact, up to the local truncation error [of $O(\Delta x^2)$, where Δx is the spatial grid discretization step that enters the numerical computation].

This is shown for the case of the DB solitary wave in Fig. 1, where we have fixed the parameters $g_{11} = 1$ (this means that $g_{ij} = \tilde{g}_{ij}$) and $g_{22} = 0.95$ to the ones relevant for ^{87}Rb; furthermore, the coefficient g_{12} is initialized weakly on the immiscibile side at $g_{12} = 0.975$ (as is relevant for this atomic gas), and the variation of the relevant solution is followed over the range of parameters $g_{12} \in [0.975, 1]$. To confirm that as the interspecies interaction is varied the analytical solution is followed, we have used—as the simplest nontrivial diagnostic—the amplitude of the bright component A_2 (for A_1 the agreement is naturally excellent, but trivial, as there is no functional dependence). This is shown in the left panel of the figure, with the numerical results given by the solid line, while the analytical expression of Eq. (14) is shown by the dashed one. On the other hand, the right panel illustrates the nature of the variation of the solution as the limit of vanishing amplitude is approached; in this case, this limit is $g_{12} = g_{11}$, since $g_{11} > g_{22}$ and the dark soliton is in the component with the largest scattering length. For increasing g_{12} approaching g_{11}, the width of the dark soliton decreases and, together with it, the width of the "trapped" bright soliton bound state also decreases. In addition, the amplitude of the bright soliton [proportional to $\sqrt{g_{11} - g_{12}}$ according to Eq. (14)] also decreases and tends to 0 at the relevant limit. It should be noted here that not only the amplitude A_2 but also the full spatial form of the solutions shown on the right panel has been found to be in excellent agreement with the theoretical prediction. This is expected since the two only differ due to the local truncation error of $O(\Delta x^2)$ of the numerical method.

Similar diagnostics but now in the case of the soliton lattices are shown in Figs. 2 and 3. The former presents the sn-cn solutions, where the bright lattice bears out-of-phase nearest neighbors, while the latter concerns the sn-dn case with the bright solitons being all in-phase.

2. *Single DB soliton in the presence of a trap*

Our other analytical prediction concerns Eq. (56) providing a prediction for the frequency of oscillation of a DB soliton in the presence of a parabolic trap. While the equation more generally connects the DB motion through an effective mass to the gradient of the trapping potential, in the present setting we will restrict our considerations to the linear restoring force in the case of a harmonic trap. To examine the validity of this prediction, we find the numerically exact (up to the prescribed

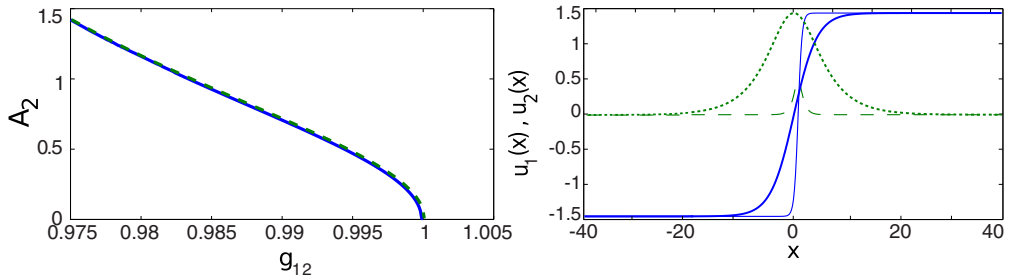

FIG. 1. (Color online) A prototypical example of the comparison of the solution obtained analytically as a function of continuation in g_{12} for fixed $g_{11} = 1$ and $g_{22} = 0.95$, starting with the relevant parameters for ^{87}Rb of $g_{12} = 0.975$ and approaching the limit of $g_{12} \to g_{11}$. The comparison made here concerns the amplitude A_2 of the bright soliton. The dashed line contains the analytical prediction of Eq. (14), while the solid line is the fully numerical result obtained as a result of a fixed point iteration in a grid of spacing $\Delta x = 0.2$. The very slight (nearly imperceptible) disparity stems from local truncation error [of $O(\Delta x^2)$] of the numerical method. The right panel contains the numerically obtained (but matching the analytical up to the local truncation error) dark-bright soliton for $g_{12} = 0.975$ (thicker lines; solid for the dark and dashed for the bright) and for $g_{12} = 0.995$ (thinner lines).

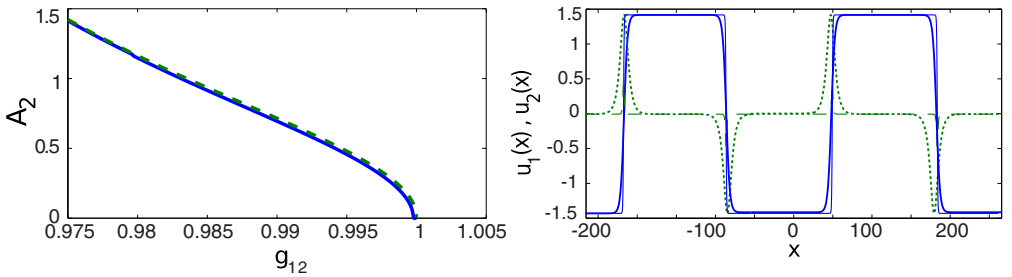

FIG. 2. (Color online) The same diagnostics as for the single dark-bright soliton of Fig. 1 are used but now for the case of the sn-cn solution branch.

accuracy discussed above) solitary wave for different values of g_{12} (we now fix μ_d and μ_b, while varying g_{12}) and compare the spectrum of the linearization around it with the frequency predicted by Eq. (56). As argued in our earlier work (see, e.g., [7] for $g_{ij} = 1$), the spectrum of the linearization around a DB solitary wave should contain an anomalous, so-called negative energy mode with a frequency associated with the oscillational frequency of the DB within the parabolic trap. Indeed, as is confirmed by Fig. 4, such a frequency is present in this case as well and is found to be in very good agreement with our theoretical prediction for this motion in the interval $g_{12} \in [0,2]$. However, for lower values of the parameter, a progressive discrepancy between the theoretical prediction and the numerical result can be discerned, e.g., for $g_{12} < 0.8$.

In an attempt to appreciate the origin of this discrepancy, we illustrate the form of the solution as g_{12} is decreased in Fig. 5. From these findings, it is immediately evident that while our DB ansatz correctly captures the relevant waveform near and beyond the threshold for immiscibility, it is far less adequate in describing the solitary wave on the miscible side. There, the miscible interaction with the dark component rapidly widens the bright counterpart (see especially the top left panel of the figure for $g_{12} = 0.6$), clearly illustrating the inadequacy of our hyperbolic secant waveform. This naturally justifies the interval of good agreement between the theoretical and numerical oscillation frequency result.

B. Further numerical findings

We now explore more broadly the nature of the solitary DB waves and of the lattices thereof both in the absence and in the presence of the trap for features and regimes which are not captured by our analytical considerations.

In Fig. 6, we now fix the values of the chemical potentials (at $\mu_d = 1.5$ and $\mu_b = 1.23$, and g_{22} will be set to 0.95 for computations hereafter) and vary the value of g_{12} from 0.8 (top left) to 0.9 (top right), to 1.1 (bottom left) to 1.3 (bottom right). We can see that even in this region of g_{12} which is outside the range of our analytically tractable lattice solutions of the sn-cn type, such solutions can still be retrieved numerically. In the immiscible regime, the solutions consist of thin DB solitons, wherein the bright components of the pair alternate in phase. The immiscibility leads the bright component to lie very close to 0 density in between its spikes due to the strong mutual repulsion with the finite density (in these intermediate regions) dark component. However, as the miscible limit is approached and eventually traversed, while the dark component does not change significantly, the bright component broadens considerably and starts approaching a more "trigonometric" rather than "hyperbolic secant" type shape between its local maxima and minima.

We subsequently also examined the linearization (so-called Bogolyubov–Cde Gennes or BdG) spectrum around such a periodic solution, in order to identify the stability of these states. The conclusions of our analysis are shown in Fig. 7. The spectrum is obtained with two methods. The first one, shown in the left panel, concerns the direct eigenvalue computation of the linearization matrix around the exact periodic solution that is obtained from our Newton-Raphson method (with finite differences applied for the spatial discretization). The second plot of the right panel "enhances" this spectrum by considering the so-called Hill's method [26], taking direct advantage of the fact that the solution is periodic to resolve more adequately the perturbation wave numbers associated with the unit cell of its periodicity. This enhancement of the finite difference method by its combination with the Hill method has been described in

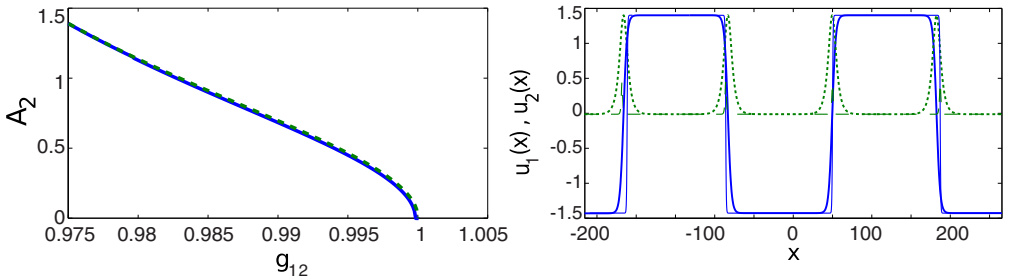

FIG. 3. (Color online) The same diagnostics as for the single dark-bright soliton of Fig. 1 are used but now for the case of the sn-dn solution branch.

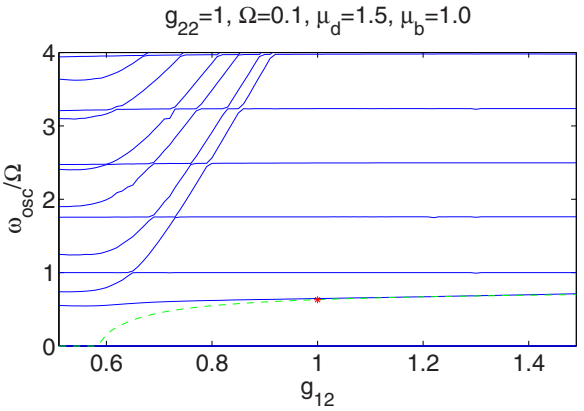

FIG. 4. (Color online) The figure shows the numerical oscillation frequency through BdG analysis (blue solid lines) versus the analytical predictions using the Hamiltonian perturbation theory in Eq. (56) (green dashed line), while the red star represents the prediction from [3] for $g_{11} = g_{12} = g_{22} = 1$. Here $g_{22} = 1$, $\Omega = 0.1$, $\mu_d = 1.5$, $\mu_b = 1.0$, and $dx = 0.001$. Notice that the spectrum in addition to this anomalous mode of oscillation, bears a large number of modes (nearly flat) associated with the dark component and a similarly large number of modes associated with the bright component (bearing a rapid variation). The theoretical prediction for the anomalous mode is very good roughly for $g_{12} \in [0.8,2]$, while it becomes progressively worse for lower parameter values.

[26] and is directly applied here. We can see that the spectrum contains as a part the linearization spectrum of the left panel, but also fills in additional eigenvalues due to its ability to more finely probe the perturbation wave numbers in comparison to the standard finite difference scheme. The details of Hill's method are described in the Appendix.

The relevant conclusions are also interesting from a physical point of view. It can already be seen from the imaginary parts of the relevant eigenfrequencies that there is a drastic change of the eigenvalue behavior and of their relative frequency spacing as the miscible threshold is approached. However, more critically for our stability purposes, we can observe that there is an interval of g_{12}'s in the vicinity of the

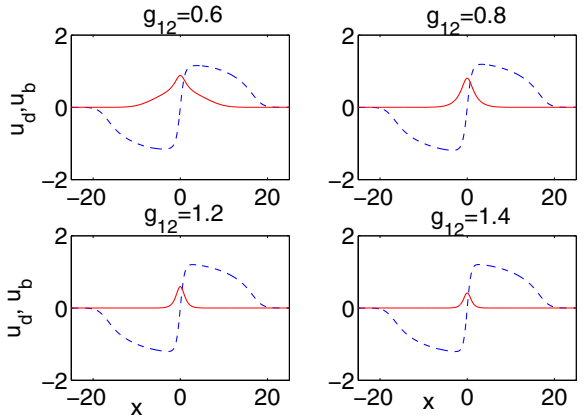

FIG. 5. (Color online) This shows the profile of the (single wave) stationary solution for different g_{12}. The parameters are the same as in Fig. 4.

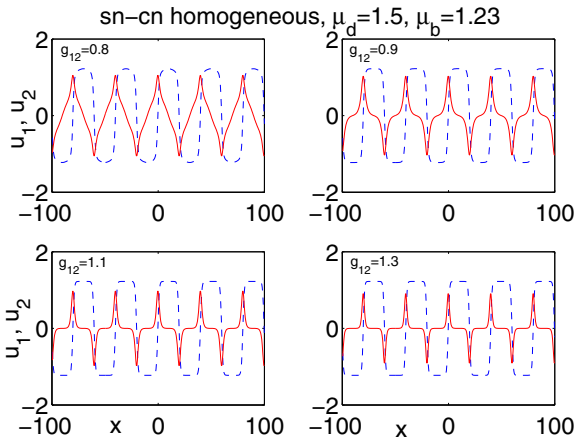

FIG. 6. (Color online) The figure shows the stationary profile of the sn-cn-type periodic solution for $g_{12} = 0.8, 0.9, 1.1, 1.3$ on the top left, top right, bottom left, and bottom right panel, respectively. The chemical potentials used are $\mu_d = 1.5$ and $\mu_b = 1.23$.

miscibility-immiscibility threshold, and especially so weakly on the immiscible side (i.e., for $1 < g_{12} < 1.2$ or so), where the relevant periodic solution is *least unstable*. We should remind the reader that in the Hamiltonian system considered herein, instability (at the linearization level) arises whenever an eigenmode exists with $\mathrm{Re}(\lambda) \neq 0$. Hence, the potential manipulation of the relevant interspecies interaction coefficient would be most likely to produce such long-lived solutions on the weakly immiscible side.

Similar results, still without a trap (i.e., in the homogeneous BEC realm) are shown for the lattice solution where the bright solitons are in-phase (the sn-dn lattice) in Fig. 8. This solution is also found to exist for more general conditions than the ones for which it is traced analytically earlier. Here, we fix $\mu_d = 1.5$ and $\mu_b = 0.975$ and again vary g_{12}. Again a variation is discernible as the miscibility-immiscibility threshold is traversed to wider bright solitary waves, while on the immiscible side these are well separated and far narrower. The stability is again computed with the two methods (finite difference method for the linearization eigenvalue computation and also its variant incorporating the Hill's approach). As is shown in Fig. 9, once again there appears a minimal growth rate (and hence a maximal life time of the pertinent waveforms) to be applicable weakly on the immiscible side (yet fairly closely to the miscibility-immiscibility threshold). As one proceeds deeper on the immiscible or for that matter on the miscible side, the solutions become more strongly unstable and hence less likely to be observable even transiently.

An additional comment is due here. Given that both the sn-cn and our sn-dn solutions presented above are generally unstable with $\mathrm{Re}(\lambda) > 0$, a natural follow-up question becomes that of their lifetime (and hence of their potential experimental observability). A typical ballpark estimate of this sort can be obtained by the time of the instability manifestation, a typical estimate of which is given by $1/\mathrm{Re}(\lambda)$, respectively, for each of these solutions. Based on this quantity and the rescaling of time according to $\omega_\perp^{-1}$, one can then obtain a lifetime estimate in dimensional units. For instance, assuming a transverse trapping frequency $\omega_\perp = 2\pi \times 80$ Hz, the instability growth

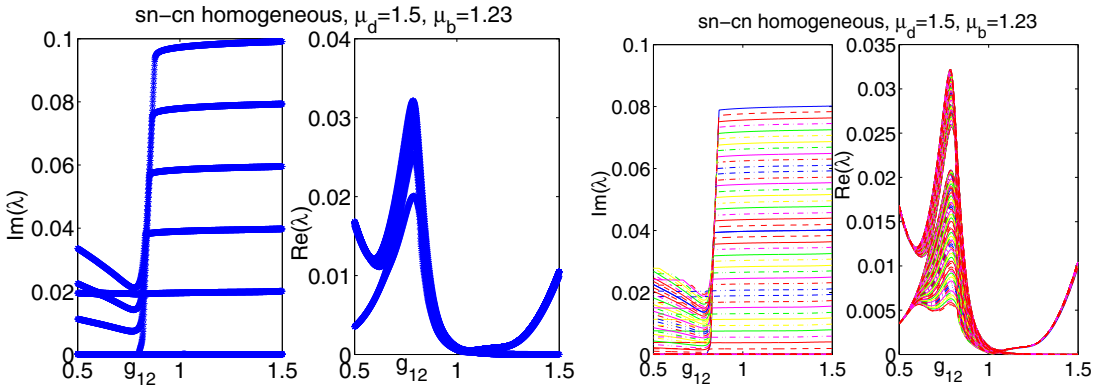

FIG. 7. (Color online) The left panel shows the spectrum of the sn-cn periodic solution as a function of g_{12} for $\mu_d = 1.5$ and $\mu_b = 1.23$ using a finite difference method. The right panel shows the same spectrum, but also when applying the so-called Hill's method (using different wave numbers through imposing a suitable phase θ at the edge of a single period and considering—in this case 11—different values of θ).

rate of 0.02 which appears as the rough minimum for the sn-dn waveform per the right panel of Fig. 9 corresponds to a lifetime of about 100 ms. In the case of the sn-cn solution of Fig. 7, the corresponding minimum appears to be approximately around one order of magnitude lower, hence assuming a $\mathrm{Re}(\lambda) = 0.002$, we can infer lifetimes of the order of about 1 s. Both of these are certainly within the realm of experimental observability (and adequate temporal resolution) with current imaging techniques. A similar procedure can be used for the trapped variants of the waveforms examined below.

We now turn to the consideration of trapped variants of the lattice solutions, as an extension of both the single DB trapped solution, but also the homogeneous BEC lattices of sn-cn and sn-dn waveforms. Our numerical computations for the two types of lattices are shown, respectively, in Figs. 10 and 11. In Fig. 10, we can observe the persistence of the sn-cn lattice in the presence of the trap, although an intriguing byproduct of the interplay between the presence of a finite $\Omega \neq 0$ and a progressively stronger interspecies interaction g_{12} is the gradual depletion of the outer bright peaks, eventually (see bottom right for $g_{12} = 1.3$) in favor of a single peak at the center. The stability results again illustrate that even in the presence of the trap the instability growth rates of the solution are again minimal in the vicinity of the miscibility-immiscibility threshold (although in this case, the absolute minimum of the growth rates appears to be shifted towards the weakly miscible side). Fairly similar conclusions, both as regard the "squeezing" (and eventual elimination) of the bright peaks, as well as the minimal growth rates on the weakly miscible side can be observed also for the trapped variant of the sn-dn solution in Fig. 11.

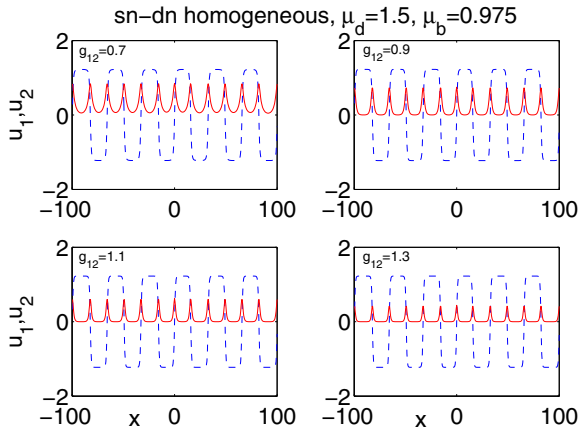

FIG. 8. (Color online) This shows the stationary profile of the sn-dn-type periodic solution for $g_{12} = 0.7, 0.9, 1.1, 1.3$ on the top left, top right, bottom left, and bottom right panel, respectively. The chemical potentials are $\mu_d = 1.5$ and $\mu_b = 0.975$. For $g_{12} < 0.7$ when it is small enough, we see the dn solutions will no longer touch the x axis, but rather "lift up" above it.

IV. CONCLUSIONS AND FUTURE CHALLENGES

In the present work, we have revisited the theme of dark-bright solitary waves in atomic Bose-Einstein condensates. We have considered such nonlinear structures in the presence of general interaction coefficients, motivated by the tunability of the scattering lengths, by means of Feshbach resonances which, in turn, permit a tunability of the intra- and interspecies effective nonlinear interaction coefficients in the mean-field picture. We have seen that remarkably the DB states in the presence and absence of the trap persist for a very broad range of interspecies interactions (this has been our principal control parameter). Within a suitably narrow range, we have been able to predict such a variation even analytically. We have also analytically predicted the motion of these DB solitary waves, identifying it as a harmonic oscillation within a parabolic trap. However, we have also gone well beyond individual dark-bright solitary waves, and have explored extended variants thereof, in the form of DB soliton lattices. Such lattices were predicted analytically in the form of cnoidal wave solutions with the bright components forming adjacent in-phase or out-of-phase pairs, i.e., sn-dn and sn-cn solutions, respectively. While these solutions were found in the homogeneous BEC, it was possible to computationally extend them even in the trapped case. Finally, their stability was also numerically explored, finding that they can be least unstable in the vicinity of the miscibility-immiscibility threshold.

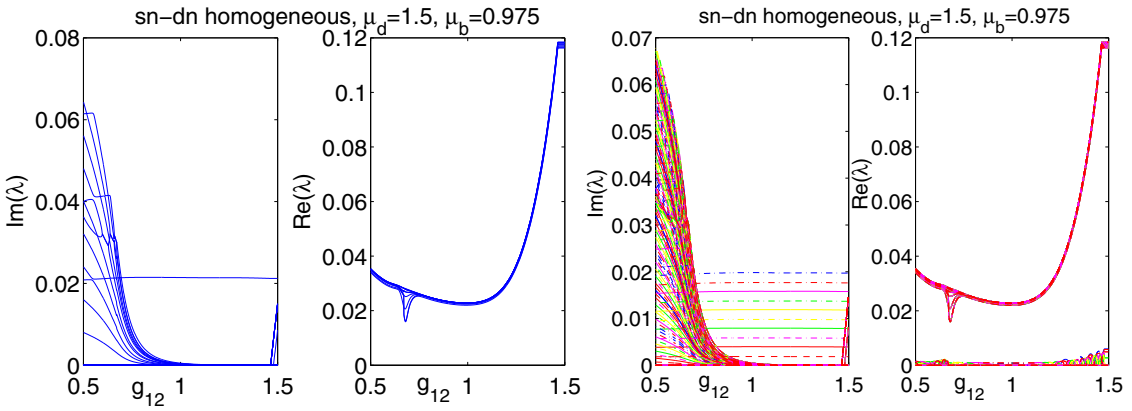

FIG. 9. (Color online) The left panel shows the spectrum of the sn-dn periodic solution for $\mu_d = 1.5$ and $\mu_b = 0.975$ as a function of g_{12} using the finite difference method. The right panel once again shows the same spectrum but with the Hill's method (for 11 values of the relevant angle θ) incorporated in the computation. The relevant waveform is generically unstable, although it is most weakly so on the slightly immiscible side.

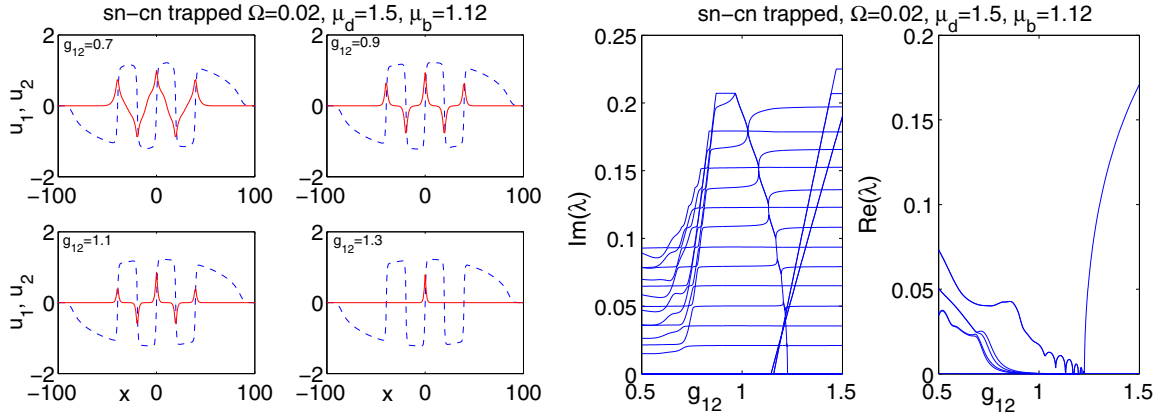

FIG. 10. (Color online) The left panel of the figure shows the stationary profile of trapped sn-cn-type solutions for $g_{12} = 0.7, 0.9, 1.1, 1.3$ on the top left, top right, bottom left, and bottom right panel, respectively. The trapping frequency is $\Omega = 0.02$, while the chemical potentials are $\mu_d = 1.5$ and $\mu_b = 1.12$. When g_{12} is about 1.2, it is interesting to note that the combination of the trap and the immiscibility only permits to one of the bright peaks (the central one) to persist, while the rest have disappeared. The right panel shows the linearization spectrum (again, imaginary and real parts) as a function of g_{12}.

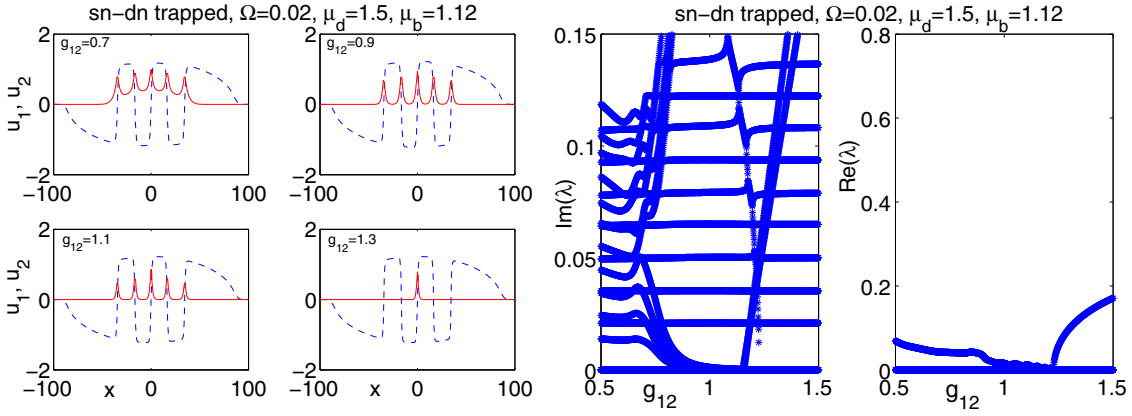

FIG. 11. (Color online) The left panel shows the stationary profile of sn-dn-type solutions in the presence of a trap, for $g_{12} = 0.7, 0.9, 1.1, 1.3$ on the top left, top right, bottom left, and bottom right panel, respectively. The trap frequency is $\Omega = 0.02$ and the chemical potentials are $\mu_d = 1.5$ and $\mu_b = 1.12$. The right panel again shows the corresponding linearization eigenvalues as a function g_{12}.

Given the extensive level of control of recent experiments on multicomponent, DB-soliton-bearing experiments (see, for instance, [4–7,10–12]) and the ability to tune scattering lengths by means of the Feshbach resonance mechanism [17], we believe that the type of states and configurations proposed herein should be well within experimental reach. Additionally, it would be extremely interesting to generalize relevant configurations in higher dimensions. So far, to the best of our knowledge, only configurations of a single or two [14,15] vortex-bright states have been proposed and the pertinent understanding of their dynamics is purely numerical. Obtaining an analytical description of their motion and generalizing such states in the realm of lattices would be a particularly interesting possibility in its own right, in a way perhaps reminiscent of other types of multicomponent lattices (of vortex molecules) such as the ones proposed in Ref. [27]. Relevant studies are currently in progress and will be reported in future publications.

APPENDIX: FINITE DIFFERENCE, FINITE DIFFERENCE WITH HILL AND HILL'S METHOD

In order to determine the linear stability of the stationary solution $(u_{1,0},u_{2,0})$, we assume a general perturbation around it in the form,

$$u_d = u_{1,0} + \epsilon[a(x)e^{\lambda t} + b(x)^* e^{\lambda^* t}], \tag{A1}$$

$$u_b = u_{2,0} + \epsilon[c(x)e^{\lambda t} + d(x)^* e^{\lambda^* t}], \tag{A2}$$

and substitute in the dynamical equations, computing only the $O(\epsilon)$ corrections. The relevant linear eigenvalue problem is then written as

$$\lambda \begin{pmatrix} a \\ b \\ c \\ d \end{pmatrix} = \begin{pmatrix} A_{11} & A_{12} & A_{13} & A_{14} \\ A_{21} & A_{22} & A_{23} & A_{24} \\ A_{31} & A_{32} & A_{33} & A_{34} \\ A_{41} & A_{42} & A_{43} & A_{44} \end{pmatrix} \begin{pmatrix} a \\ b \\ c \\ d \end{pmatrix},$$

where λ, (a,b,c,d) are the eigenvalues and eigenvectors, respectively. In particular, the matrix elements are

$$A_{11} = -\tfrac{1}{2}\partial_{xx} - \mu_d + V(x) + 2g_{11}|u_{1,0}|^2 + g_{12}|u_{2,0}|^2, \tag{A3}$$

$$A_{22} = -A_{11}, \tag{A4}$$

$$A_{33} = -\tfrac{1}{2}\partial_{xx} - \mu_b + V(x) + 2g_{22}|u_{2,0}|^2 + g_{12}|u_{1,0}|^2, \tag{A5}$$

$$A_{44} = -A_{33}, \tag{A6}$$

$$A_{12} = g_{11}u_{1,0}^2, \tag{A7}$$

$$A_{13} = g_{12}u_{1,0}u_{2,0}^*, \tag{A8}$$

$$A_{14} = g_{12}u_{1,0}u_{2,0}, \tag{A9}$$

$$A_{21} = -A_{12}^*, \tag{A10}$$

$$A_{23} = -A_{14}^*, \tag{A11}$$

$$A_{24} = -A_{13}^*, \tag{A12}$$

$$A_{31} = A_{13}^*, \tag{A13}$$

$$A_{32} = A_{14}, \tag{A14}$$

$$A_{34} = g_{22}u_{2,0}^2, \tag{A15}$$

$$A_{41} = -A_{22}^*, \tag{A16}$$

$$A_{42} = -A_{32}, \tag{A17}$$

$$A_{43} = -A_{34}. \tag{A18}$$

Now we briefly discuss two methods for studying the above linear eigenvalue problem. For the finite difference method, we discretize the eigenvector and the Jacobian matrix, i.e., work with the grid $x_n = x_1 + (n-1)\Delta x$. For the eigenvectors (a,b,c,d), we then have $a(x) = [a(x_1),a(x_2),\ldots,a(x_n)]$, $b(x) = [b(x_1),b(x_2),\ldots,b(x_n)]$, $c(x) = [c(x_1),c(x_2),\ldots,c(x_n)]$, and $d(x) = [d(x_1),d(x_2),\ldots,d(x_n)]$. The resulting matrix eigenvalue-eigenvector problem can thus be numerically solved.

For the finite difference method with Hill's method incorporated [26], we select a number of values for $\theta \in [0,2\pi)$, and make the following changes based on the finite difference method,

$$A_{11}(1,n) \to A_{11}(1,n)e^{i\theta}, \tag{A19}$$

$$A_{22}(1,n) \to A_{22}(1,n)e^{i\theta}, \tag{A20}$$

$$A_{33}(1,n) \to A_{33}(1,n)e^{i\theta}, \tag{A21}$$

$$A_{44}(1,n) \to A_{44}(1,n)e^{i\theta}, \tag{A22}$$

$$A_{11}(n,1) \to A_{11}(n,1)e^{-i\theta}, \tag{A23}$$

$$A_{22}(n,1) \to A_{22}(n,1)e^{-i\theta}, \tag{A24}$$

$$A_{33}(n,1) \to A_{33}(n,1)e^{-i\theta}, \tag{A25}$$

$$A_{44}(n,1) \to A_{44}(n,1)e^{-i\theta}. \tag{A26}$$

Then we evaluate the eigenvalues and eigenvectors of the matrix A over a period of the periodic solution of interest and superpose the relevant spectra obtained for different values of θ.

In the present work, we computed the spectrum with finite differences and finite differences incorporating Hill's method (over a period) and confirmed the agreement between the two. When computing the spectrum with finite differences, only a finite number of periods is used (due to the finiteness of the computational domain needed to be employed), as is, e.g., shown for our sn-cn and sn-dn solutions, in the absence of a trap. On the other hand, in the case of the Hill's method with finite differences, a finite number of values of θ is used within the same period. In that light, the asymptotic limit where the two methods would be equivalent would be that of infinitely many phase factors in the Hill's method (with finite differences) and, correspondingly, infinitely many periods in the true solution within the standard finite difference method. Nevertheless, a glimpse of the correspondence of the results of

the two solutions is given by our results here, i.e., in Figs. 7 and 9. Notice that, e.g., on the imaginary axis of the corresponding sn-cn and sn-dn spectral plots, we only see a small fraction of the spectrum, which in its fullness encompasses the entire imaginary axis. As an additional alternative, one may also consider the direct Hill's method as described, e.g., in [26].

[1] S. V. Manakov, Zh. Eksp. Teor. Fiz. **65**, 505 (1973) [Sov. Phys. JETP **38**, 248 (1973)].

[2] M. J. Ablowitz, B. Prinari, and A. D. Trubatch, *Discrete and Continuous Nonlinear Schrdinger Systems* (Cambridge University Press, Cambridge, 2004).

[3] Th. Busch and J. R. Anglin, Phys. Rev. Lett. **87**, 010401 (2001).

[4] C. Becker, S. Stellmer, P. Soltan-Panahi, S. Dörscher, M. Baumert, E.-M. Richter, J. Kronjäger, K. Bongs, and K. Sengstock, Nature Phys. **4**, 496 (2008).

[5] S. Middelkamp, J. J. Chang, C. Hamner, R. Carretero-González, P. G. Kevrekidis, V. Achilleos, D. J. Frantzeskakis, P. Schmelcher, and P. Engels, Phys. Lett. A **375**, 642 (2011).

[6] C. Hamner, J. J. Chang, P. Engels, and M. A. Hoefer, Phys. Rev. Lett. **106**, 065302 (2011).

[7] D. Yan, J. J. Chang, C. Hamner, P. G. Kevrekidis, P. Engels, V. Achilleos, D. J. Frantzeskakis, R. Carretero-González, and P. Schmelcher, Phys. Rev. A **84**, 053630 (2011).

[8] C. Y. Yin, N. G. Berloff, V. M. Pérez-García, D. Novoa, A. V. Carpentier, and H. Michinel, Phys. Rev. A **83**, 051605 (2011).

[9] V. A. Brazhnyi and V. M. Pérez-García, Chaos, Solitons and Fractals **44**, 381 (2011).

[10] M. A. Hoefer, J. J. Chang, C. Hamner, and P. Engels, Phys. Rev. A **84**, 041605 (2011).

[11] D. Yan, J. J. Chang, C. Hamner, M. Hoefer, P. G. Kevrekidis, P. Engels, V. Achilleos, D. J. Frantzeskakis, and J. Cuevas, J. Phys. B: At. Mol. Opt. Phys. **45**, 115301 (2012).

[12] A. Álvarez, J. Cuevas, F. R. Romero, C. Hamner, J. J. Chang, P. Engels, P. G. Kevrekidis, and D. J. Frantzeskakis, J. Phys. B: At. Mol. Opt. Phys. **46**, 065302 (2013).

[13] J. Stockhofe, P. G. Kevrekidis, D. J. Frantzeskakis, and P. Schmelcher, J. Phys. B: At. Mol. Opt. Phys. **44**, 191003 (2011).

[14] J. J. García-Ripoll and V. M. Pérez-García, Phys. Rev. Lett. **84**, 4264 (2000).

[15] K. J. H. Law, P. G. Kevrekidis, and L. S. Tuckerman, Phys. Rev. Lett. **105**, 160405 (2010); M. Pola, J. Stockhofe, P. Schmelcher, and P. G. Kevrekidis, Phys. Rev. A **86**, 053601 (2012).

[16] S. Inouye, M. R. Andrews, J. Stenger, H.-J. Miesner, D. M. Stamper-Kurn, and W. Ketterle, Nature (London) **392**, 151 (1998); J. L. Roberts, N. R. Claussen, J. P. Burke, Jr., C. H. Greene, E. A. Cornell, and C. E. Wieman, Phys. Rev. Lett. **81**, 5109 (1998); E. A. Donley, N. R. Claussen, S. L. Cornish, J. L. Roberts, E. A. Cornell, and C. E. Wieman, Nature (London) **412**, 295 (2001).

[17] G. Thalhammer, G. Barontini, L. De Sarlo, J. Catani, F. Minardi, and M. Inguscio, Phys. Rev. Lett. **100**, 210402 (2008); S. B. Papp, J. M. Pino, and C. E. Wieman, *ibid.* **101**, 040402 (2008).

[18] G. Csire, D. Schumayer, and B. Apagyi, Phys. Rev. A **82**, 063608 (2010).

[19] V. V. Afanasjev, E. M. Dianov, and V. N. Serkin, IEEE J. Quantum Electron. **25**, 2656 (1989).

[20] N. A. Kostov and I. M. Uzunov, Opt. Commun. **89**, 389 (1992).

[21] P. G. Kevrekidis, D. J. Frantzeskakis, and R. Carretero-González (eds.), *Emergent Nonlinear Phenomena in Bose-Einstein Condensates* (Springer-Verlag, Berlin, 2008); R. Carretero-González, D. J. Frantzeskakis, and P. G. Kevrekidis, Nonlinearity **21**, R139 (2008).

[22] A. D. Martin and J. Ruostekoski, New J. Phys. **12**, 055018 (2010).

[23] A. D. Martin and J. Ruostekoski, New J. Phys. **14**, 043040 (2012).

[24] V. Achilleos, P. G. Kevrekidis, V. M. Rothos, and D. J. Frantzeskakis, Phys. Rev. A **84**, 053626 (2011); V. Achilleos, D. Yan, P. G. Kevrekidis, and D. J. Frantzeskakis, New J. Phys. **14**, 055006 (2012).

[25] D. J. Frantzeskakis, J. Phys. A: Math. Theor. **43**, 213001 (2010).

[26] B. Deconinck and J. N. Kutz, J. Comp. Physics **219**, 296 (2006).

[27] K. Kasamatsu, M. Tsubota, and M. Ueda, Phys. Rev. Lett. **93**, 250406 (2004).